Oral presentation | Higher order methods
Higher order methods-IV
Tue. Jul 16, 2024 4:30 PM - 6:30 PM Room C

[6-C-02] Analysis of Dispersion and Dissipation Characteristics of Stabilization Methods for Discontinuous Galerkin Schemes

*Geng Liang[1], Hui Xu[1] (1. Shanghai Jiao Tong University)

Keywords: entropy stable Discontinuous Galerkin Schemes, Eigenanalysis, Spectral Vanishing Viscosity, Positivity-preserving Limiter, Jump Penalty

Twelfth International Conference on
Computational Fluid Dynamics (ICCFD12),
Kobe, Japan, July 14-19, 2024

Analysis of Dispersion and Dissipation Characteristics of Stabilization Methods for Discontinuous Galerkin Schemes

Geng Liang, Hui Xu*
School of Aeronautics and Astronautics, Shanghai Jiao Tong University
*Corresponding author: dr.hxu@sjtu.edu.cn

Abstract: This study aims to give a comprehensive analysis of current stabilization techniques for optimizing Discontinuous Galerkin (DG) methods, including spectral vanishing viscosity (SVV), positivity-preserving limiters achieved by introducing lower orders, jump penalty (JP), and filtering. Their linear characteristics are examined through eigenanalysis in conjunction with mathematical proofs and numerical calculations, while their nonlinear properties are investigated under the framework of entropy stability. By examining the influence of nodal distribution, algorithmic order, Péclet number and parameters on linear characteristics, this study summarizes the behavior of various stabilization methods at different wavenumbers and provides a basis for the parameter selection of certain methods based on dispersion relation; by analyzing entropy dissipation terms in nonlinear characteristics under the entropy-stable formulation, this study summarizes the performance of various methods on issues such as excessive dissipation.

Keywords: Discontinuous Galerkin, spectral vanishing viscosity, positivity-preserving limiter, jump penalty, filtering, eigenanalysis, entropy stability

1 Introduction

Discontinuous Galerkin (DG) methods are essential for numerically solving partial differential equations, offering high-order accuracy and flexibility with complex geometries [1]. They excel in parallel computing architectures [2] but face challenges in convection-dominated flows and hyperbolic conservation laws, often resulting in numerical instability and non-physical solutions [3]. While DG methods with smooth solutions ensure accuracy and stability [4], practical computations involving shocks and discontinuities pose stability challenges.

High-order methods often encounter instability due to the Gibbs phenomenon, which causes numerical oscillations when approximating discontinuities. Therefore, additional stabilization techniques are necessary [5]. Early stabilization techniques from spectral methods introduced exponential dissipation to the high-order energy spectrum [6], and filters were widely applied in spectral and DG methods [7, 8]. Classical stabilization strategies like WENO limiters [9], slope limiters [1], and extremum limiters [10] often cause excessive dissipation and accuracy loss as they act post-emergence of oscillations. Recent approaches apply filters directly to the differential operator to mitigate discontinuity effects earlier [11]. Spectral Vanishing Viscosity (SVV) is a powerful stabilization method using filters to generate weak solutions mathematically, allowing flexible control of viscosity strength at different orders [12]. Widely employed in spectral methods, SVV effectively suppresses numerical oscillations near shocks and improves the resolution of under-resolved features [13]. SVV emerged as an early proven tool for nonlinear problems and is extensively applied in fluid dynamics models [14]. It combines various forms of artificial viscosity to enhance solution physicality [15]. Stabilization methods must enhance stability while preserving physicality and accuracy. Physicality requires additional dissipation only where discontinuities or lack of smoothness exist, vanishing elsewhere. Methods like filtering and SVV rely on artificially set shock sensors, which may erase high-order features. A classical approach is the penalty method, initially used in spectral methods to enforce boundary conditions weakly [16, 17]. In DG formulations, the penalty method effectively exists within numerical fluxes, adding dissipation at cell boundaries [18, 19, 20]. Positivity-preserving limiters from hybrid low-order methods offer another approach, allowing limited oscillation control without entirely eliminating them [21]. These limiters use low-order algorithm solutions to limit oscillation amplitude, maintaining accuracy while controlling dissipation [22]. Early algorithms used empirical formulas for blending coefficients, while later research optimized parameters

using gradient descent methods [23]. Subcell limiters with different mixing coefficients within the same cell have also been proposed [24].

Stabilization methods for DG schemes, initially developed for handling discontinuities, are now applied to nonlinear under-resolved flows. Parameter selection, often based on empirical formulas, significantly impacts dispersion and dissipation characteristics. Eigenvalue analysis quantitatively assesses these effects on discrete systems' stability [25]. Classical DG methods have extensive eigenvalue analysis work, helping evaluate stabilization techniques' effects on eigenvalue distribution [26]. Methods like Spectral Vanishing Viscosity (SVV) [27] and Jump Penalty (JP) [28] have undergone such analysis. Recent modal analyses assess numerical diffusion in semi-discrete systems, linking it to under-resolved simulation levels [25]. These analyses quantify flow disturbances' numerical characteristics [29]. Stabilization methods for discontinuities have evolved alongside methods for managing nonlinearity, such as entropy-stable methods. Errors and under-resolution are acceptable in linear systems but problematic in hyperbolic nonlinear systems. Classical DG methods struggle with stability in approximating nonlinear convective terms due to aliasing errors, necessitating additional stability conditions. Entropy-stable methods ensure weak solutions' uniqueness and adherence to physical entropy conditions, crucial in handling shocks and discontinuities [30]. Entropy projection techniques mitigate aliasing errors by incorporating entropy variables [31]. Entropy stability has become crucial in nonlinear frameworks, guiding the development of entropy-stable formulations across methodologies [32]. Unlike discontinuity-handling methods, entropy stability applies only to nonlinear systems, aligning with energy stability in linearized systems. Stabilization methods like SVV [27] and positivity-preserving limiters [33] have corresponding entropy-stable forms. Current research focuses on dissipation, dispersion, and nonlinear characteristics in complex flows, considering parameter selection's impact. Despite some studies, systematic analysis and comparative research are lacking. This research uses eigenvalue and entropy stability analysis frameworks to systematically analyze and describe computational methods' characteristics, guiding stability method and parameter selection for complex flows.

2 Eigenanalysis framework

When tackling the numerical resolution of convection-diffusion equations, it is crucial to grasp the inherent dispersion and dissipation properties. At the heart of many physical phenomena lies the convection-diffusion equation, and its simplest, one-dimensional form is

$$u_t + au_x = \mu u_{xx}, \tag{1}$$

wherein u denotes a scalar physical quantity such as heat intensity, a denotes the velocity of convection, and μ signifies the diffusion coefficient.

The main principle of Eigenanalysis is the von-Neumann stability analysis which evaluates the responses of a numerical scheme by postulating a solution resembling $e^{i(kx-\omega t)}$ [34], where k is the spatial frequency and ω is the complex temporal frequency. The real part of ω is associated with the velocity of the waveform, whereas its imaginary part corresponds to the rate of the waveform's decay. To discern the interconnection between dispersion and dissipation, we take this assumed solution into the discretized variant of the equation, which results in the relationship:

$$\omega = ak - i\mu k^2.$$

This expression sheds light on two key aspects: firstly, the real part, encapsulated as ak, reveals that the wave's velocity is intrinsically linked to the convection speed a, ensuring that the numerical solution is free from additional dispersion inaccuracies; secondly, the imaginary part, denoted by $-i\mu k^2$, delineates the rate at which the wave's amplitude reduces. This indicates that the damping is proportional to the square of the spatial frequency. Therefore, it is evident that as the frequency increases, the wave's amplitude undergoes faster attenuation due to the effects of numerical diffusion.

when performing eigenanalysis on the semi-discrete form of the DG method, we consider the number of nodes within an element as the degree of freedom, resulting in the linear system $-i\omega\mathbf{u} = \mathbf{H}\mathbf{u}$, where $\mathbf{u} = (u_0, \ldots, u_N)^T$ is the solution vector, N is the order of the solution polynomial. Furthermore, the semi-discrete problem can be expressed as the following eigenvalue problem:

$$\det(\mathbf{H} + i\omega\mathbf{I}) = 0 \tag{2}$$

where $(\omega h)_{\mathcal{R}} = -2\mathcal{I}(\lambda)$ reflect dispersion property, while$(\omega h)_{\mathcal{I}} = 2\mathcal{R}(\lambda)$reflect dissipation property.

The matrix form of the nodal DG method for the convection-diffusion equation is as follows:

$$\frac{h}{2}\mathbf{W}\frac{\partial \mathbf{u}}{\partial t} = \mathbf{Q}_h^T(a\mathbf{u} - \mu\mathbf{q}) - \mathbf{E}^T\mathbf{B}(\hat{\mathbf{f}} - \hat{\mathbf{f}}_v), \quad \frac{h}{2}\mathbf{W}\mathbf{q} = -\mathbf{Q}_h^T\mathbf{u} + \mathbf{E}^T\mathbf{B}\hat{\mathbf{u}} \tag{3}$$

where $\mathbf{W}_{mn} = (\phi_m, \phi_n)_{\widetilde{I}}$ is an orthogonal diagonal mass matrix in nodal form according to Gaussian integral, and $(\mathbf{Q}_h)_{mn} = (\frac{\partial \phi_m}{\partial x}, \phi_n)_{\widetilde{I}}$ is a nodal form stiffness matrix. $\mathbf{E} = [\ \mathbf{E}_- \quad \mathbf{E}_+\ ]^T$, where $\mathbf{E}_-$ and $\mathbf{E}_+$ are interpolation vectors projecting from the nodes to the left and right edges. $\mathbf{B}$ is the edge integral matrix, which is equal to $diag(-1, 1)$ in a one-dimensional problem. Due to the Summation-By-Parts (SBP) property of the DG scheme[35], $\mathbf{Q}_h^T + \mathbf{Q}_h^T = \mathbf{E}^T\mathbf{B}\mathbf{E}$. $\hat{\mathbf{f}}, \hat{\mathbf{f}}_v, \hat{\mathbf{u}}$ are the numerical fluxes. In this paper, we use upwind flux for $\hat{f}$ and local discontinuous Galerkin method(LDG) for $\hat{f}_v, \hat{u}$[36]. In eigenanalysis, solution vectors which belong to the elements I_{j-1}, I_{j+1} located on the left and right of I_j are defined as

$$u|_{I_{j-1}} = u|_{I_j}\, e^{-ikh}, \quad u|_{I_{j+1}} = u|_{I_j}\, e^{ikh} \tag{4}$$

Therefore, the linear system of a DG scheme can be expressed as:

$$\frac{h}{2a}\frac{\partial \mathbf{u}}{\partial t} = \mathbf{H}\mathbf{u}, \quad \mathbf{H} = -\mathbf{D}(\lambda) + \frac{2}{Pe}\mathbf{D}(-\lambda_a)\mathbf{D}(\lambda_a) \tag{5}$$

where λ, λ_a are upwind coefficients for the main and the auxiliary equations, $Pe = ah/\mu$ is Péclet number, and $\mathbf{D}$ is a first-order derivative matrix expressed as:

$$\mathbf{D}(\lambda) = \mathbf{W}^{-1}\mathbf{Q}_h + \frac{1}{2}\mathbf{W}^{-1}\mathbf{E}^T(\mathbf{I}_2 - \lambda\mathbf{B}) \begin{bmatrix} \mathbf{E}_- - \mathbf{E}_+ e^{-ikh} \\ \mathbf{E}_- e^{ikh} - \mathbf{E}_+ \end{bmatrix} \tag{6}$$

When filter stabilization methods are added to the DG scheme[6], the form is as follows:

$$\mathbf{H}^* = \mathbf{V}_q\mathbf{F}\mathbf{P}_q\mathbf{H} \tag{7}$$

where $\mathbf{V}_q, \mathbf{P}_q$ are the projection matrices for the nodal and the modal to convert to each other ($\mathbf{V}_q\mathbf{P}_q = \mathbf{I}$). $\mathbf{F}$ is a diagonal matrix, whose coefficient determines the proportion of energy retained by each mode after filtering. For spectral vanishing viscosity method[12], the linear system comes to

$$\mathbf{H}^* = \mathbf{H} + \frac{2}{Pe^*}\mathbf{D}\mathbf{V}_q\mathbf{F}_{SVV}\mathbf{P}_q\mathbf{D} \tag{8}$$

where $\mathbf{F}_{SVV}$is a diagonal matrix, whose coefficient determines the intensity of artificial dissipation in each mode. Pe^* is a new Péclet number corresponding to the artificial viscosity coefficient.For SVV, we can add the following artificial dissipation terms to the right-hand side of (**??**):

$$\mu_a(\mathbf{Q}_h\mathbf{f}_v + \mathbf{E}^T\mathbf{B}[\![\mathbf{f}_{v,f}]\!]) \qquad \mathbf{f}_v = \mathbf{L}_q^T\sqrt{\mathbf{D}}(\mathbf{V}_q\mathbf{F}_{SVV}\mathbf{P}_q) * \sqrt{\mathbf{D}}\mathbf{L}_q\mathbf{q}_v \qquad \mathbf{W}\mathbf{q}_v = \mathbf{Q}_h\mathbf{v} + \mathbf{E}^T\mathbf{B}[\![\mathbf{v}_f]\!] \tag{9}$$

where $\mathbf{L}_q^T\mathbf{D}\mathbf{L}_q$ is the orthogonal decomposition corresponding to the Jacobi matrix of the viscous term, and $*$ represents the vanishing process. Therefore, the additional entropy on a single element is

$$\frac{\partial \Delta S}{\partial t} = \mu_a(\mathbf{v}^T\mathbf{Q}_h\mathbf{f}_v + \mathbf{v}_f^T\mathbf{B}[\![\mathbf{f}_{v,f}]\!]) = \mu_a(\mathbf{v}_f^T\mathbf{B}\mathbf{f}_{v,f} - \mathbf{v}^T\mathbf{Q}_h^T\mathbf{f}_v + \mathbf{v}_f^T\mathbf{B}[\![\mathbf{f}_{v,f}]\!]) = \mu(\mathbf{v}_f^T\mathbf{B}\bar{\mathbf{f}}_{v,f} - \mathbf{f}_v^T\mathbf{W}\mathbf{q}_v + \mathbf{f}_{v,f}\mathbf{B}[\![\mathbf{v}_f]\!]) \tag{10}$$

After summation over the entire computational domain, we obtain

$$\sum \frac{\partial \Delta S}{\partial t} = -\sum \mu_a \mathbf{f}_v^T\mathbf{W}\mathbf{q}_v \tag{11}$$

Since the Jacobi matrix from $\mathbf{q}_v$ to $\mathbf{f}_v$ generated by the physical viscosity terms possesses positive definite, and the core vector of SVV directly acts on the core vector after orthogonal decomposition, the total entropy generated is evidently negative. SVV differs from general entropy-stable methods by directly providing entropy dissipation within the cell while generally maintaining conservation at the interfaces, which makes it an important means of controlling numerical oscillations within high-order elements.

Positivity-preserving scheme is a linear combination of high-order and low-order methods[24, 37]. Here, the low-order method uses a sub-cell finite volume scheme, where the numerical fluxes used by both convective and viscous terms are consistent with DG methods. The result is a linear system as

follows:

$$\mathbf{H}^* = (1-\alpha)\mathbf{H}+\alpha\left[-\mathbf{D}^*(\lambda)+\frac{2}{Pe}\mathbf{D}^*(0)\mathbf{D}^*(0)\right], \quad \mathbf{D}^*(\lambda)=\mathbf{W}^{-1}\begin{bmatrix} \lambda & \frac{1-\lambda}{2} & & & -\frac{1+\lambda}{2}e^{-ikh} \\ -\frac{1+\lambda}{2} & \lambda & \frac{1-\lambda}{2} & & \\ & \ddots & \ddots & \ddots & \\ & & -\frac{1+\lambda}{2} & \lambda & \frac{1-\lambda}{2} \\ \frac{1-\lambda}{2}e^{ikh} & & & -\frac{1+\lambda}{2} & \lambda \end{bmatrix} \tag{12}$$

where α is the blending coefficient. It can be constant for a single element, where the limiter reduces to a classical element-wise form; alternatively it can be a matrix, where the limiter is in a sub-cell node-wise form. Next, we operate on the right-hand side of entropy-stable method to implement stabilization techniques that possess entropy-stable characteristics. First, for the positivity-preserving limiter, we obtain

$$\frac{\partial S}{\partial t} = \mathbf{v}^T\mathbf{W}((1-\alpha)\frac{\partial \mathbf{u}_H}{\partial t}+\alpha\frac{\partial \mathbf{u}_L}{\partial t}) \tag{13}$$

It is provable that entropy stability exists for both low-order and high-order method, their total entropy decreases steadily, and their additional entropy production is entirely dependent on the amount of low-order method added. For a subcell positivity-preserving limiter with a diagonal blending coefficient $\mathbf{A}$, entropy stability is also ensured as

$$\sum\frac{\partial S}{\partial t} = \mathbf{v}^T\mathbf{W}((\mathbf{I}-\mathbf{A})\frac{\partial \mathbf{u}_H}{\partial t}+\mathbf{A}\frac{\partial \mathbf{u}_L}{\partial t}) = \mathbf{v}^T\mathbf{W}\frac{\partial \mathbf{u}_H}{\partial t}+\mathbf{v}^T\mathbf{W}\mathbf{A}(\frac{\partial \mathbf{u}_L}{\partial t}-\frac{\partial \mathbf{u}_H}{\partial t}) \tag{14}$$

Since lower-order methods produce significantly higher entropy in regions where limiters are needed, an additional entropy is$\frac{\partial \Delta S}{\partial t} = \mathbf{v}^T\mathbf{W}\mathbf{A}(\frac{\partial \mathbf{u}_L}{\partial t}-\frac{\partial \mathbf{u}_H}{\partial t})$.

Jump penalty method additionally impose overupwinding ($\lambda > 1$) or extra gradient-form dissipation on element boundaries, gradient jump penalty (GJP)[18, 19] has the form as follows:

$$\mathbf{H}^* = \mathbf{H}(\sigma_s)+\sigma_g\mathbf{W}^{-1}(\mathbf{E}\mathbf{W}^{-1}\mathbf{Q}_h)^T\mathbf{B}\begin{bmatrix} \mathbf{E}_- - \mathbf{E}_+e^{-ikh} \\ \mathbf{E}_-e^{ikh}-\mathbf{E}_+ \end{bmatrix}\mathbf{D}(\lambda_a) \tag{15}$$

where $\sigma_s = \lambda - 1$ is the over-upwinding coefficient, and σ_g is a dimensionless penalty coefficient.For jump penalty method, the following gradient penalty term is added to the right-hand side of (**??**)

$$\sigma_g(\mathbf{E}\mathbf{W}^{-1}\mathbf{Q}_h)^T[\![\mathbf{q}_{v,f}]\!] \qquad \mathbf{q}_v = \mathbf{W}^{-1}(\mathbf{Q}_h\mathbf{v}+\mathbf{E}^T\mathbf{B}[\![\mathbf{v}_f]\!]) \tag{16}$$

Therefore, the additional entropy on a single element is

$$\frac{\partial \Delta S}{\partial t} = \sigma_g\mathbf{v}^T(\mathbf{E}\mathbf{W}^{-1}\mathbf{Q}_h)^T[\![\mathbf{q}_{v,f}]\!] = \sigma_g[\![\mathbf{q}_{v,f}]\!]^T\mathbf{E}(\mathbf{q}_v-\mathbf{E}^T\mathbf{B}[\![\mathbf{v}_f]\!]) \tag{17}$$

After summation over the entire computational domain, we obtain

$$\sum\frac{\partial \Delta S}{\partial t} = -\sum\sigma_g[\![\mathbf{q}_{v,f}]\!]^T[\![\mathbf{q}_{v,f}]\!] \tag{18}$$

The results indicate that with a negative gradient jump penalty coefficient, the system can produce positive additional throughput, which confirms that a positive coefficient is more conducive to stability. However, since it is entirely dependent on the boundary discontinuities, careful choice of σ_g still improves the algorithm's performance while ensuring that the entire system remains entropy stable.

3 Eigenanalysis result

3.1 Results for the DG scheme with filter

Traditionally, the stabilization of DG methods is realized through a simple filtering mechanism; its effectiveness solely hinges on the choice of an appropriate filter kernel vector. Now we want the resulting matrix to maintain an optimal balance that conserves the high-order system's integrity while bolstering the system's robustness against instability. We delve into an analysis of two distinct kernel vector

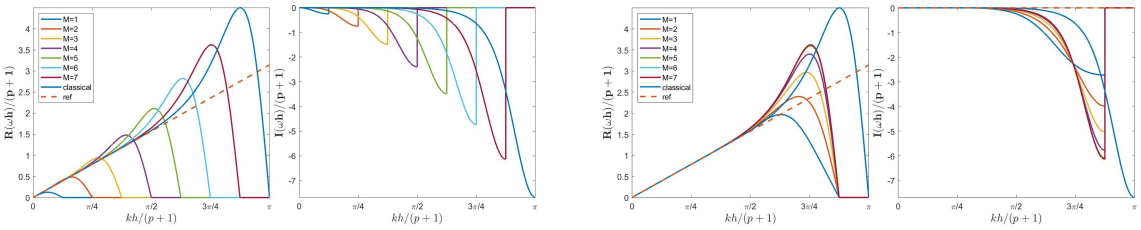

(a) step (b) trail

Figure 1: dispersion and dissipation curves for a DG scheme with filter , where $p = 7$, inviscid, using Gauss-Legendre nodes

configurations: the step function

$$F_k = \begin{cases} 0 & k > M \\ 1 & k \leq M \end{cases} \tag{19}$$

and the trailing function

$$F_k = \begin{cases} e^{-\alpha\left(\frac{k-M}{p-M}\right)^{2p}} & k > M \\ 1 & k \leq M \end{cases} \tag{20}$$

where M denotes the cutoff threshold for the filter, below which the modes remain unaffected, $\alpha = -\log(\epsilon)$, ϵ representing the machine accuracy.

By comparing the performance of these kernel vectors, as illustrated in Fig.1, we observe that the step form kernel vector takes an abrupt plunge to zero in both dispersion and dissipation curves at the designated cutoff wavenumbers. The root of this behavior lies in the obliteration of high-order system characteristics—a stark singularity that is inherently detrimental to the computational fidelity we strive for. In contrast, the trailing form kernel vector demonstrates a smooth and continuous evolution except the highest mode. Notice that the function values do not precipitously approach zero as k approaches p, which highlights that a judiciously designed filter must conserve a substantial fraction of the high-order modes. For filters, using Joint-mode analysis is more convenient. Although jump filters cannot be effectively decomposed due to their singularity, the more commonly used trial filters can obtain better high-wave number characteristics compared to primary mode analysis. Due to the fact that step filters cause zero eigenvalues, resulting in singularities, it is not possible to extract the joint-mode curves by decomposing in the direction of eigenvectors. This insight sheds light on the parallels between DG methods and other finite element strategies such as the Flux Reconstruction (FR) technique, as researchers state that the FR method can be viewed as a DG strategy equipped with a conceptual filter [38].

3.2 Results for the DG scheme with spectral vanishing viscosity

For the vanishing viscosity method, we primarily analyze the distribution pattern of artificial viscosity across different polynomial orders and the impact of the viscosity coefficient. Our discussion is based on the inviscid flow with polynomial order $p = 7$ and the use of Gauss-Legendre nodes. We recognize that the presence of artificial viscosity, when expressed as a linear combination independent of the actual viscosity, does not alter the initial findings, irrespective of any variation in the Péclet number.

Artificial viscosity is allocated following the pattern outlined by the $\mathbf{F}_{SVV}$ matrix, which is diagonally structured within the modal space. Our aim is to apply artificial viscosity to higher-order modes, but meanwhile keep it to stay minimal for lower-order modes and absent from the principal mode, so that the intrinsic characteristics of the linear system can be preserved. Normally we resort to kernel vectors such as the step function[12, 39, 40]:

$$F_k = \begin{cases} 1 & k > M \\ 0 & k \leq M \end{cases} \tag{21}$$

the trail function:

$$F_k = \begin{cases} e^{-\frac{(k-p)^2}{(k-M)^2}} & k > M \\ 0 & k \leq M \end{cases} \tag{22}$$

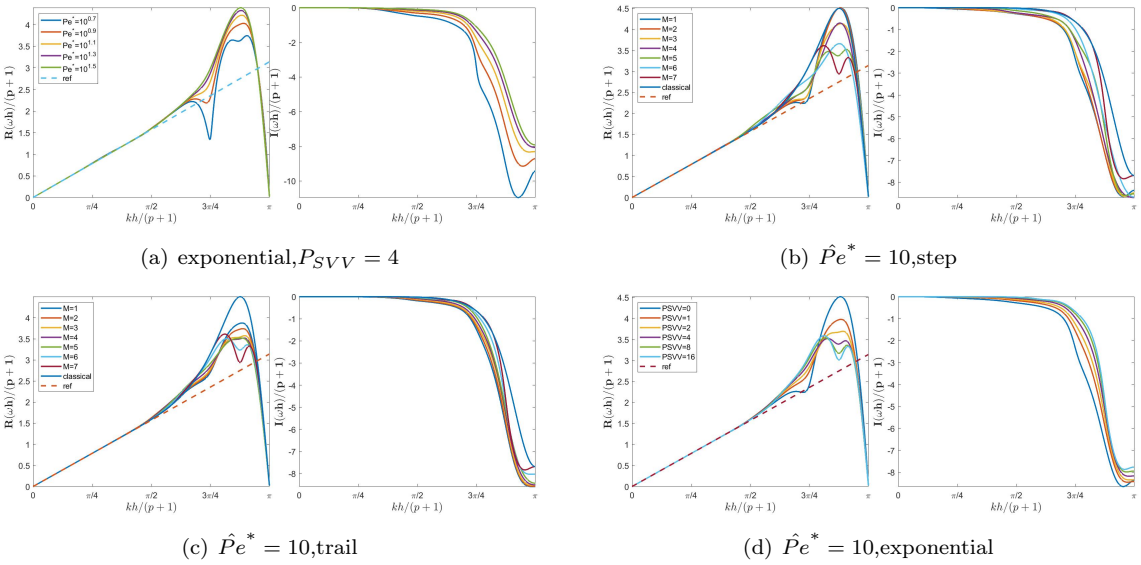

(a) exponential,$P_{SVV} = 4$ (b) $\hat{Pe}^* = 10$,step

(c) $\hat{Pe}^* = 10$,trail (d) $\hat{Pe}^* = 10$,exponential

Figure 2: dispersion and dissipation curves for a DG scheme with SVV , where $p = 7$, inviscid, using Gauss-Legendre nodes

and the exponential function:

$$F_k = \left(\frac{k}{p}\right)^{P_{SVV}} \tag{23}$$

where M denotes the cutoff level below which modes are exempt from artificial viscosity. The non-negative filtering parameter P_{SVV} defaults to a step function with a threshold of 1 when set to 0.

In Figure 2, the patterns of a linear system equipped with Spectral Vanishing Viscosity (SVV) are presented, showcasing the effects of assorted artificial viscosity configurations over a range of modes. It is evident that the artificial Péclet numbers mirror the behavior of their real viscosity counterparts in every scenario. Regarding the dispersion traits, increased levels of artificial viscosity apparently lead to a minor divergence from the baseline values at lower wavenumbers; this divergence becomes further pronounced and approaches the reference values as the wavenumbers increase. As for the dissipative traits, artificial viscosity significantly amplifies energy loss throughout the wavenumber spectrum. When considering the shape of the kernel vectors, the step form introduces distinct modal variations at various wavenumbers; it is contingent upon the filter threshold, in contrast with the continuous variations observed with the exponential form. The trailing form operates in an intermediate manner, between the step and exponential forms.

An exponential viscosity distribution is often preferable due to its ability to induce gradual changes in the system's dissipation curve. Following this, we delve into the optimal selection of artificial viscosity coefficients within the spectral viscosity elimination framework. In a linearized context, the introduction of artificial viscosity coefficients will invariably lead to deviations from the standard physical dispersion values. To grasp the full scope of this phenomenon, we explore a range of artificial Péclet numbers from 0.1 to 100, in conjunction with different filter parameters. This is reflected as a sudden jump at the corresponding wavenumber within the dissipation curve. Displayed in Fig.3 is the curve of the total variation Δ^*, indicating that even minimal high-order viscosity addition can skew the system away from the dispersion reference values. When implementing strong viscosity to smooth out irregularities, there is an optimal artificial Péclet number that can reduce the total variation to about 10^{-5}. This finding illuminates the local minima as valuable indicators for parameter selection.

To quantitatively approximate the theoretical diffusion curves, we implement the "1% rule" [41], which defines the modified wavenumber $k_{1\%} = \frac{kh}{p+1}$ as the point where the error relative to the theoretical value reaches 1%. The wavenumber linked to this error determines the region $|k_{1\%} - k_{theo}| \leq 0.01|k_{theo}|$, indicating the well-resolved range in simulation. We present the range of well-resolved scales according to the 1% rule under different parameters. For dispersion properties, the $k_{1\%}$ rapidly converges to $\pi/2$ as the artificial viscosity coefficient decreases. The difference between different kernel vectors' performance lies in their behavior at higher viscosity coefficients; exponential parameter characteristics are relatively smooth, while step-wise ones exhibit significant jumps. It is noteworthy that when the exponential

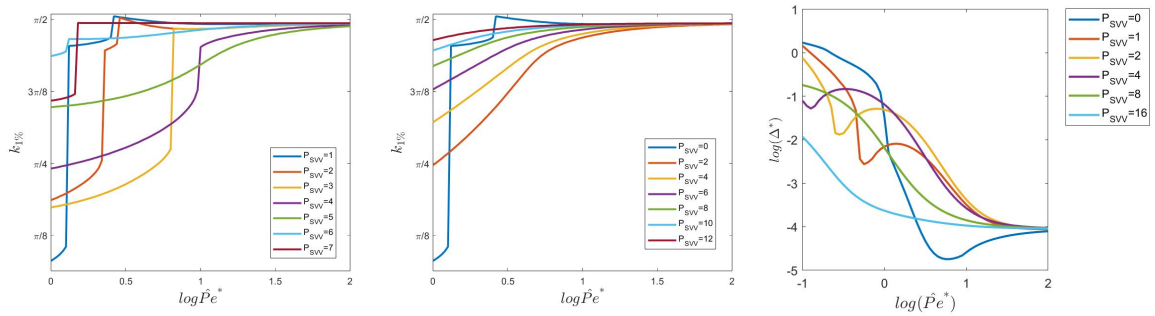

(a) 1%rule for dispersion(step) (b) 1%rule for dispersion(exponential) (c) variation for dispersion(exponential)

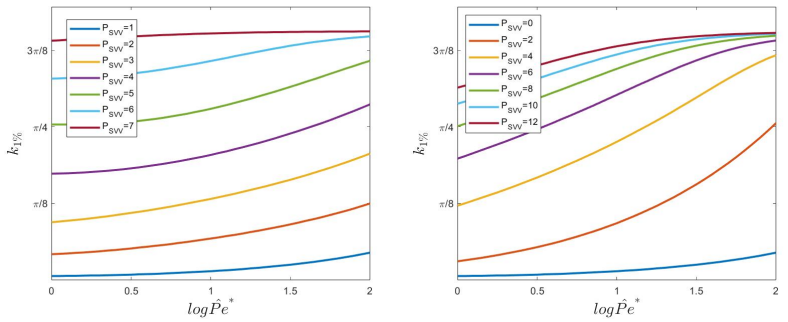

(d) 1%rule for dissipation(step) (e) 1%rule for dissipation(exponential)

Figure 3: dispersion and dissipation characteristics for a DG scheme with different artificial Péclet numbers, where $p = 7$,inviscid, using Gauss-Legendre nodes

parameter $P_{SVV} = 0$, the kernel function degenerates into a step-wise form. Regarding dissipation properties, for physical Peclet number, even with a very small viscosity coefficient, corresponding to a larger artificial Peclet number $\hat{P}e = 10$, $k_{1\%}$ is still unable to converge to the desired limit wavenumber of $3\pi/8$, and this characteristic is independent of the choice of kernel vector. These phenomena also support our variation analysis, which considers the bias of the numerical scheme's dispersion relation from the theoretical value in the range of $[0, \pi/2]$, while the stabilization method exhibits an overly dissipative behavior. Therefore, it is impossible to optimize the dissipation characteristics simultaneously with the dispersion properties.

3.3 Results for the DG scheme with positivity-preserving limiter

The method for preserving positivity within the numerical solution is accomplished through the integration of a low order total variation diminishing (TVD) scheme. This study employs a sub-cell finite element scheme that relies on upwind flux for solving the primary equation and central flux for the supplementary equation. As previously discussed, the coefficients used for this blending process can be either uniform values or variable matrices along the diagonal. The outcomes of the characteristic analysis displayed in Fig.4 illustrate the behavior under various conditions set by the blending coefficients. The results consistently show that regardless of the choice of coefficients, the resultant curve invariably resides within the bounds set by the lower and higher order method, which indicates a linear amalgamation of the two. Such a finding suggests the possibility of identifying a sub-cell approach that would allow the dispersion characteristics to align more closely with the desired physical benchmarks.

For cases involving particular orders and node distributions, we can employ convex optimization techniques to determine the blending coefficients for the sub-cells that lead to an optimal solution. These coefficients are tailored to minimize the variation in dispersion and result in more accurate and stable numerical simulations. The DG method's ability to blend low-order limiters plays a crucial role in controlling the dispersion and dissipation characteristics of the solution, ensuring that it adheres to the physical accuracy required for reliable computational predictions. Using the 1% rule, the sub-cell positivity-preserving limiter shows superior performance. Thanks to the adjustability of the parameters, it is easy to make the wavenumber $k_{1\%}$of the dispersion curve surpass $\pi/2$ and even $5\pi/8$. After specifically iterating for optimal dispersion performance, we find that under certain extreme parameters, this

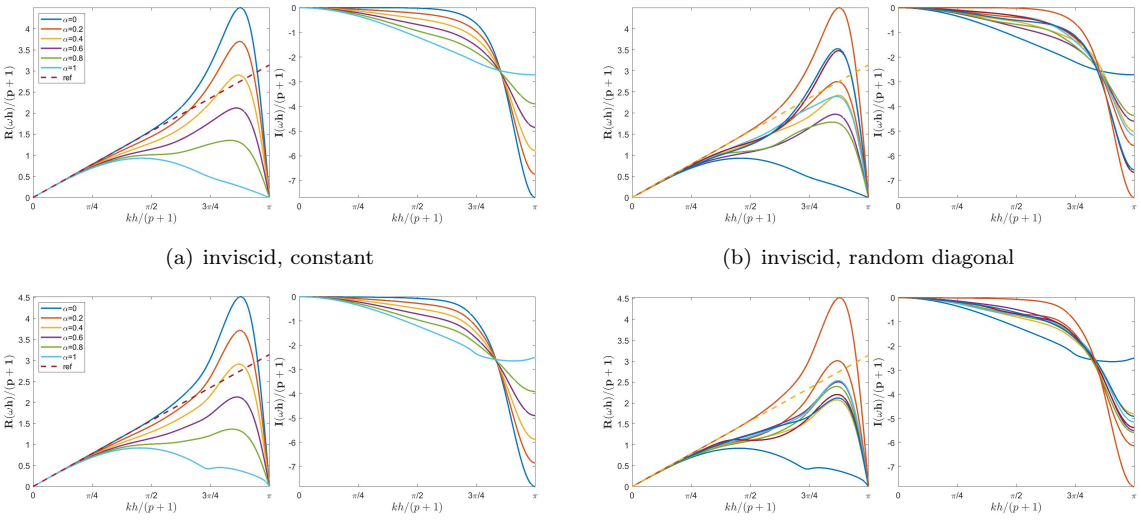

(a) inviscid, constant

(b) inviscid, random diagonal

(c) $\hat{Pe} = 50$,constant

(d) $\hat{Pe} = 50$,random diagonal

Figure 4: dispersion and dissipation curves for a DG scheme with different blending coefficient, where $p = 7$, using Gauss-Legendre nodes

value can exceed $3\pi/4$, fully demonstrating the potential of this method.

3.4 Results for the DG scheme with jump penalty

The Jump Penalty (JP) technique plays a crucial role by harnessing the gradient and upwind terms as stabilizing agents that complement each other. Our analysis delves into the dispersion and dissipation properties of σ_s, σ_g, as depicted in Fig.5. We observe that the upwind term is influential at two specific high wavenumber nodes, albeit has less impact at low wavenumbers. Our findings suggest that employing a negative gradient jump penalty coefficient can enhance the dispersion at lower wavenumbers and simultaneously mitigate dissipation, while maintaining stability at the higher wavenumber spectrum.

The gradient coefficient's behavior is defined by three nodal points, with one notably approaching $\pi/2$. Our data shows that when using one of the higher positive gradient coefficients, the dissipation curve begins to show positive values, which is a clear signal of instability. Moreover, the necessity for larger gradient penalty values escalates with increasing Péclet numbers. The results demonstrate that a negative gradient jump penalty coefficient can draw both dispersion and dissipation curves closer to the reference values at high wavenumbers, while a positive gradient jump penalty coefficient brings the curves and reference values closer at lower wavenumbers and exhibits stronger dissipation at higher wavenumbers.

We further scrutinize the deviations in dispersion curves from the benchmark for varying solution penalty coefficients and gradient penalty coefficients, as illustrated in Fig.6. Certainly, suitable gradient penalty coefficients are consistently positive, and the magnitude of the solution penalty coefficient correlates with the degree of excessive upwinding. The latter necessitates a more pronounced gradient dissipation term to achieve equilibrium. This observation underscores the increased dissipation and serves as a cautionary note on the potential for excessive upwinding within the jump penalty approach, emphasizing the need to adapt to the convective nature of the flow. Notice that a negative gradient jump penalty coefficient may cause positive dissipation in the dissipation curve at high wavenumbers. Although a negative coefficient seems to bring the dispersion curve overall closer to the reference value, total variation analysis tells that within the range of $[0, \pi/2]$, the penalty coefficients that make the curve closest to the reference value are positive. In the analysis using the 1% rule, we find that unless a significantly large negative upwind coefficient is chosen, the $k_{1\%}$ stays near $\pi/2$. A properly selected, smaller negative penalty coefficient can expand the range in which the algorithm is well-resolved; however, once the penalty coefficient becomes too large, the characteristics of the algorithm deteriorate rapidly. Moreover, the larger is the excessive upwind coefficient, the more caution is needed for the choice of negative penalty coefficient.

In conclusion, the JP method in the DG framework requires a nuanced balance between the penalty coefficients to optimize the numerical stability and accuracy, reflecting the intricate interplay between

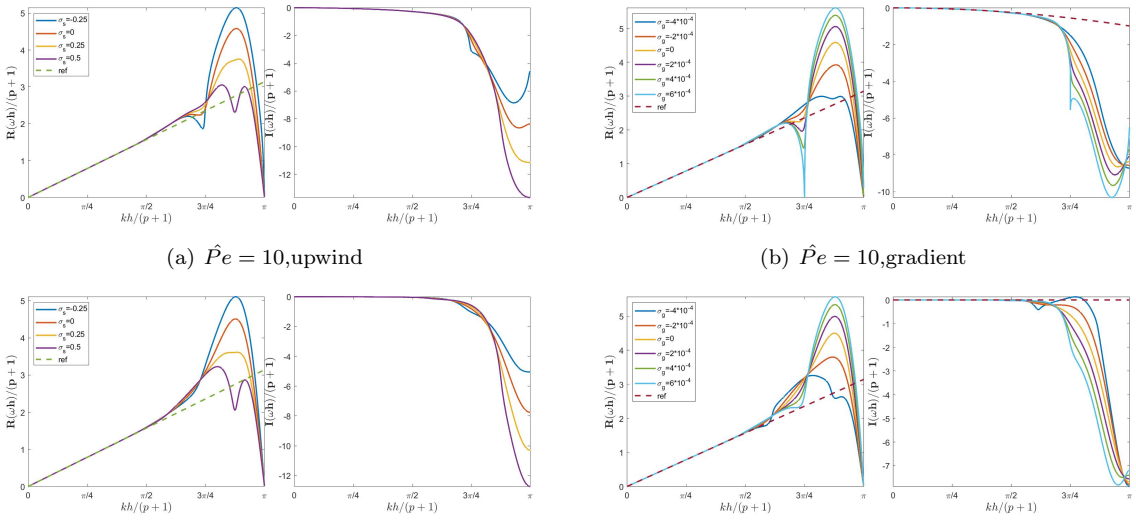

(a) $\hat{Pe} = 10$,upwind (b) $\hat{Pe} = 10$,gradient

(c) inviscid, upwind (d) inviscid, gradient

Figure 5: dispersion and dissipation curves for a DG scheme with different penalty parameter, where $p = 7$, using Gauss-Legendre nodes

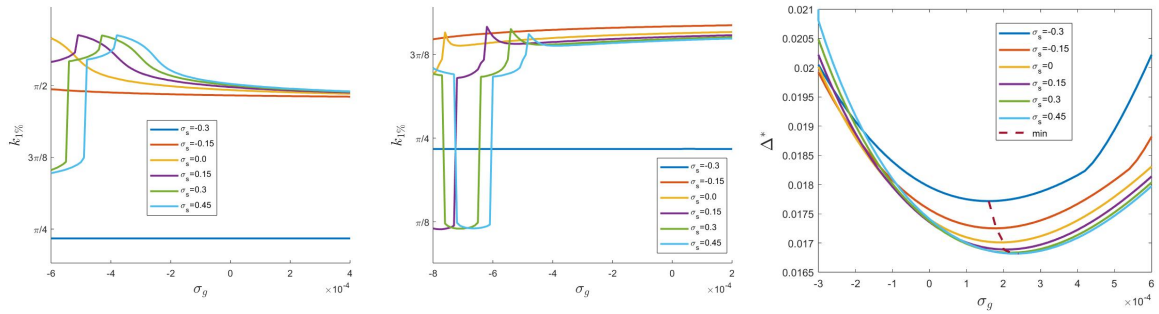

(a) 1%rule for dispersion (b) 1%rule for dispersion (c) variation for dispersion

Figure 6: dispersion and dissipation characteristics for a DG scheme with different solution penalty coefficients and gradient penalty coefficients, where $p = 7, \hat{Pe} = 100$, using Gauss-Legendre nodes

dispersion, dissipation, and the convective dynamics inherent in the system.

4 Conclusion

In conclusion, we conduct a comprehensive evaluation of various stabilization techniques within the Discontinuous Galerkin scheme, scrutinize their behavior across a spectrum of wavenumbers, and validate these observations through numerical computations. A structured approach to parameter selection based on the analysis of dispersion and dissipation is promoted, and thereby provides a foundational framework for optimizing DG methods. We also use entropy-stable formulations to particularly focus on the management of entropy dissipation in relation to nonlinear characteristics, which not only advances the understanding of the stabilization mechanisms but also enhances these techniques' accuracy and stability in the numerical simulation of complex fluid scenarios. The subcell positivity limiter is characterized by its adaptability, with its dispersion and dissipation traits fully determined by blending coefficients and strictly bounded by the features of high and low-order methods; the SVV method stands out for its ability to introduce significant dissipation across all wavenumbers without adversely affecting dispersion properties; the jump penalty method uniquely optimizes both dispersion and dissipation in certain low-order domains, although careful control of its coefficients is essential to maintain entropy stability; filtering is highlighted with it particular limitations in the excessive loss of high-wavenumber features leading to dispersion errors, and its challenges in ensuring entropy stability, which may precipitate premature computational failures. We look for further research on how various stabilization techniques may

resolve specific demands in complex fluid simulations and make advancements in numerical analysis and engineering.

References

[1] Jan S Hesthaven and Tim Warburton. *Nodal discontinuous Galerkin methods: algorithms, analysis, and applications*. Springer Science & Business Media, 2007.

[2] Bernardo Cockburn and Chi-Wang Shu. The runge–kutta discontinuous galerkin method for conservation laws v: multidimensional systems. *Journal of computational physics*, 141(2):199–224, 1998.

[3] Bernardo Cockburn. Discontinuous galerkin methods for convection-dominated problems. In *High-order methods for computational physics*, pages 69–224. Springer, 1999.

[4] Albert Romkes, S Prudhomme, and JT Oden. A priori error analyses of a stabilized discontinuous galerkin method. *Computers & Mathematics with Applications*, 46(8-9):1289–1311, 2003.

[5] Franco Brezzi, Bernardo Cockburn, L Donatella Marini, and Endre Süli. Stabilization mechanisms in discontinuous galerkin finite element methods. *Computer Methods in Applied Mechanics and Engineering*, 195(25-28):3293–3310, 2006.

[6] Heinz-Otto Kreiss and Joseph Oliger. Stability of the fourier method. *SIAM Journal on Numerical Analysis*, 16(3):421–433, 1979.

[7] David Gottlieb and Jan S Hesthaven. Spectral methods for hyperbolic problems. *Journal of Computational and Applied Mathematics*, 128(1-2):83–131, 2001.

[8] Jan Hesthaven and Robert Kirby. Filtering in legendre spectral methods. *Mathematics of Computation*, 77(263):1425–1452, 2008.

[9] Jianxian Qiu and Chi-Wang Shu. Runge–kutta discontinuous galerkin method using weno limiters. *SIAM Journal on Scientific Computing*, 26(3):907–929, 2005.

[10] Jan S Hesthaven. *Numerical methods for conservation laws: From analysis to algorithms*. SIAM, 2017.

[11] Jennifer K Ryan and Bernardo Cockburn. Local derivative post-processing for the discontinuous galerkin method. *Journal of Computational Physics*, 228(23):8642–8664, 2009.

[12] Eitan Tadmor. Convergence of spectral methods for nonlinear conservation laws. *SIAM Journal on Numerical Analysis*, 26(1):30–44, 1989.

[13] Gui Qiang Chen, Qiang Du, and Eitan Tadmor. Spectral viscosity approximations to multidimensional scalar conservation laws. *Mathematics of Computation*, 61(204):629–643, 1993.

[14] Robert M Kirby and Spencer J Sherwin. Stabilisation of spectral/hp element methods through spectral vanishing viscosity: Application to fluid mechanics modelling. *Computer methods in applied mechanics and engineering*, 195(23-24):3128–3144, 2006.

[15] Juan Manzanero, Esteban Ferrer, Gonzalo Rubio, and Eusebio Valero. Design of a smagorinsky spectral vanishing viscosity turbulence model for discontinuous galerkin methods. *Computers & Fluids*, 200:104440, 2020.

[16] Lucia Dettori and Baolin Yang. On the chebyshev penalty method for parabolic and hyperbolic equations. *ESAIM: Mathematical Modelling and Numerical Analysis*, 30(7):907–920, 1996.

[17] Jan S Hesthaven. A stable penalty method for the compressible navier–stokes equations: Ii. one-dimensional domain decomposition schemes. *SIAM Journal on Scientific Computing*, 18(3):658–685, 1997.

[18] Jiaqing Kou, Oscar A Marino, and Esteban Ferrer. Jump penalty stabilization techniques for under-resolved turbulence in discontinuous galerkin schemes. *Journal of Computational Physics*, 491:112399, 2023.

[19] Rodrigo C Moura, Andrea Cassinelli, André FC da Silva, Erik Burman, and Spencer J Sherwin. Gradient jump penalty stabilisation of spectral/hp element discretisation for under-resolved turbulence simulations. *Computer Methods in Applied Mechanics and Engineering*, 388:114200, 2022.

[20] Erik Burman and Alexandre Ern. Continuous interior penalty hp-finite element methods for advection and advection-diffusion equations. *Mathematics of computation*, 76(259):1119–1140, 2007.

[21] Xiangxiong Zhang. On positivity-preserving high order discontinuous galerkin schemes for compressible navier–stokes equations. *Journal of Computational Physics*, 328:301–343, 2017.

[22] Yimin Lin, Jesse Chan, and Ignacio Tomas. A positivity preserving strategy for entropy stable discontinuous galerkin discretizations of the compressible euler and navier-stokes equations. *Journal of Computational Physics*, 475:111850, 2023.

[23] François Vilar. A posteriori correction of high-order discontinuous galerkin scheme through subcell

finite volume formulation and flux reconstruction. *Journal of Computational Physics*, 387:245–279, 2019.

[24] Andrés M Rueda-Ramírez, Will Pazner, and Gregor J Gassner. Subcell limiting strategies for discontinuous galerkin spectral element methods. *Computers & Fluids*, 247:105627, 2022.

[25] Irving E Reyna Nolasco, Aimad Er-Raiy, Radouan Boukharfane, Anwar A Aldhafeeri, Lisandro Dalcin, and Matteo Parsani. Eigenanalysis and non-modal analysis of collocated discontinuous galerkin discretizations with the summation-by-parts property. *Computers & Mathematics with Applications*, 124:196–217, 2022.

[26] Gianmarco Mengaldo, RC Moura, B Giralda, J Peiró, and SJ Sherwin. Spatial eigensolution analysis of discontinuous galerkin schemes with practical insights for under-resolved computations and implicit les. *Computers & Fluids*, 169:349–364, 2018.

[27] Rodrigo Costa Moura, Spencer J Sherwin, and Joaquim Peiró. Eigensolution analysis of spectral/hp continuous galerkin approximations to advection–diffusion problems: Insights into spectral vanishing viscosity. *Journal of Computational Physics*, 307:401–422, 2016.

[28] Rodrigo C Moura, A da Silva, Erik Burman, and Spencer J Sherwin. Eigenanalysis of gradient-jump penalty (gjp) stabilisation for cg. Technical report, Tech. rep., Technical report. https://doi.org/10.13140/RG. 2.2. 32887.85924, 2020.

[29] Rodrigo C Moura, Pablo Fernandez, Gianmarco Mengaldo, and Spencer J Sherwin. Temporal eigenanalysis of hdg methods for linear advection-diffusion. Technical report, Research report, Instituto Tecnológico de Aeronáutica, 2018.

[30] Jesse Chan. On discretely entropy conservative and entropy stable discontinuous galerkin methods. *Journal of Computational Physics*, 362:346–374, 2018.

[31] Jesse Chan, Hendrik Ranocha, Andrés M Rueda-Ramírez, Gregor Gassner, and Tim Warburton. On the entropy projection and the robustness of high order entropy stable discontinuous galerkin schemes for under-resolved flows. *Frontiers in Physics*, 10:898028, 2022.

[32] Juan Manzanero, Gonzalo Rubio, David A Kopriva, Esteban Ferrer, and Eusebio Valero. An entropy–stable discontinuous galerkin approximation for the incompressible navier–stokes equations with variable density and artificial compressibility. *Journal of Computational Physics*, 408:109241, 2020.

[33] Tarik Dzanic and Freddie D Witherden. Positivity-preserving entropy-based adaptive filtering for discontinuous spectral element methods. *Journal of Computational Physics*, 468:111501, 2022.

[34] Charles Hirsch. Chapter 7-consistency, stability and error analysis of numerical schemes. *Numerical Computation of Internal and External Flows (Second Edition), second edition Edition, Butterworth-Heinemann, Oxford*, pages 283–335, 2007.

[35] David C Del Rey Fernández, Jason E Hicken, and David W Zingg. Review of summation-by-parts operators with simultaneous approximation terms for the numerical solution of partial differential equations. *Computers & Fluids*, 95:171–196, 2014.

[36] Jue Yan and Chi-Wang Shu. Local discontinuous galerkin methods for partial differential equations with higher order derivatives. *Journal of Scientific Computing*, 17:27–47, 2002.

[37] Andrés M Rueda-Ramírez and Gregor J Gassner. A subcell finite volume positivity-preserving limiter for dgsem discretizations of the euler equations. *arXiv preprint arXiv:2102.06017*, 2021.

[38] Y Allaneau and Antony Jameson. Connections between the filtered discontinuous galerkin method and the flux reconstruction approach to high order discretizations. *Computer Methods in Applied Mechanics and Engineering*, 200(49-52):3628–3636, 2011.

[39] Andrés Mateo-Gabín, Juan Manzanero, and Eusebio Valero. An entropy stable spectral vanishing viscosity for discontinuous galerkin schemes: application to shock capturing and les models. *Journal of Computational Physics*, 471:111618, 2022.

[40] SM Ould Kaber. A legendre pseudospectral viscosity method. *Journal of Computational Physics*, 128(1):165–180, 1996.

[41] Rodrigo Costa Moura, Spencer J Sherwin, and Joaquim Peiró. Linear dispersion–diffusion analysis and its application to under-resolved turbulence simulations using discontinuous galerkin spectral/hp methods. *Journal of Computational Physics*, 298:695–710, 2015.